NJC

ROYAL SOCIETY OF CHEMISTRY

PAPER

View Article Online
View Journal

Cite this: DOI: 10.1039/c9nj05642d

Deciphering the positional impact of chlorine in a new series of berberine analogues towards the superb-selective "turn-on" hydrophobic signaling of bovine serum albumin at physiological pH†

Gopal Chandra Jana,[a] Sk Nayim,[a] Nandan Kumar Sahoo,[a] Somnath Das,[a] Mt Nasima Aktara,[a] Anirudha Patra,[a] Md. Maidul Islam[b] and Maidul Hossain *[a]

The optical signals of serum albumin (SA) provide precious information for realizing its native functions, in addition to developing related biomedical applications. Herein, we report a new class of easy synthesizable and water-soluble compounds (BZ_1–BZ_5) based on different chlorine positions on 9-*O*-benzyl-substituted berberine scaffolds for the selective detection of bovine serum albumin (BSA) in CP buffer solution (10 mM, pH 7.2) based on two competing factors: hydrophobic interactions and steric repulsion. The frail emission intensities of these probes were enhanced upon the addition of BSA; exceptionally, a remarkable increase in emission intensity (140-fold) and remarkable lifetime and quantum yield increases make BZ_4 an excellent fluorescence turn-on hydrophobic BSA sensor. Selectivity and co-existence studies involving other proteins, free tryptophan, *etc.* revealed that the microenvironment around the tryptophan moiety in BSA incites drastic spectral changes upon the introduction of BSA. Moreover, the most efficient lumino-probe, BZ_4, can detect bovine serum albumin at a nanomolar level (LOD = 3.3 nM) with a broadened range of linearity and slight altering of the secondary structure of the protein. Our experimental results and docking simulation studies show that the probe BZ_4 binds preferentially at "binding site II" of BSA. In addition, the binding and conformational alterations of BSA provoked by these analogues have been intensely investigated, and we fruitfully relate the binding results to the sensing outcome. The obtained results reveal how the different positioning of chlorine in benzyl-substituted berberine affects the hydrophobic sensing of BSA, making these probes a new category of BSA selective material with potential applications in proteome research.

Received 11th November 2019,
Accepted 27th December 2019

DOI: 10.1039/c9nj05642d

rsc.li/njc

1. Introduction

In recent times, the notable development of a versatile biosensor for both the unambiguous qualitative and quantitative labeling of proteins with high recognizing capabilities and good binding linearity has attracted immense interest from chemical and biochemical researchers.[1] Turn-on emission probes are valuable markers in proteomics as their emission intensities are amplified upon binding with proteins; these are mostly applicable to the quantification of specific proteins and offer enough information for the *in vivo* imaging of proteins, for realizing the roles of proteins in cellular system and, in addition, for the development of biomedical and biotechnological applications.[2] Accordingly, the design and development of new promising fluorescent sensors with high sensitivity for recognizing biomolecules is a central research area for protein biochemists due to the ample application of these sensors in pathogen detection and medical diagnosis.[3]

Proteins are involved in a number of pivotal components in living systems. Serum albumins, including bovine serum albumin (BSA) and human serum albumin (HSA), are the most plentiful carrier proteins in animal and human sera. They have been implicated in a large number of physiological processes, like maintaining blood osmotic pressure; acting as major transport proteins in blood plasma for many compounds, such as fatty acids; and being involved in initiating the transfer of various ligands crossways through organ-circulatory interfaces, such as in the kidneys, intestines, liver, and brain.[4–7] Albumins also act as covalent adducts, forming species with glutathione, cysteine, and other different metals, like Cu(II), Ni(II), and so on.[8] Anomalous levels of serum albumins are strongly related to numerous diseases, such as diabetes mellitus,[9] sepsis,[10,11]

[a] *Department of Chemistry and Chemical Technology, Vidyasagar University, Midnapore, 721102, West Bengal, India. E-mail: hossainm@mail.vidyasagar.ac.in; Tel: +91-9432976277*

[b] *Department of Chemistry, Aliah University, Kolkata, West Bengal, India*

† Electronic supplementary information (ESI) available. See DOI: 10.1039/c9nj05642d

liver injuries,[12] and kidney failure,[13] and serum albumin levels are presently viewed as diagnostic or analytical markers for various diseases.[14–16] The above facts have directed researchers to deliberate the structural aspects of serum albumins and their interactions with drugs and various small biomolecules, and to investigate the influence of albumins on the photophysical properties of the affected molecule. Structurally, serum albumins have two binding sites, *i.e.*, site I and site II, which are situated in three homologous domains forming a heart-shaped protein.[8,17] The site I binding efficacy is chiefly based on hydrophobic interactions, while site II binding includes a combination of hydrogen bonding, and electrostatic and hydrophobic interactions.[18,19] It has been reported previously that biomolecules have good binding affinity to serum albumin mostly through site II binding, and proficient photodynamic therapeutic (PDT) applications have been shown.[20,21]

Therefore, the development of proficient fluorescent probes for selective-binding protein sensors is highly necessary and, consequently, enormous efforts relating to the qualitative and quantitative monitoring of albumins in biological fluids have been reported over several decades. Various methods have been developed for albumin detection, such as immune assays, colorimetric techniques,[22–24] cyclic voltammetry,[25,26] surface-enhanced Raman scattering,[27] and chemiluminescence.[28] Of the various methods available, fluorometric sensing has received widespread consideration due to the potential for rapid analysis, high sensitivity, and good selectivity, particularly for real-time imaging *in vivo*. To date, a large number of fluorescent probes for the quantification of bovine serum albumins have been reported,[29–32] however some of them suffer from grim disadvantages such as complicated synthetic procedures.[33–35] Poor water solubility is also a factor for some fluorescent probes like PRODAN, a neutral dye; on the other hand, some probes have been designed as reactive probes (reacting with the NH_2 or SH groups in proteins) for serum albumin labeling, which distorts the electronic effects of the probes.[36–38] Furthermore, some fluorescent sensors emit in a somewhat lower wavelength region and it is not easy to reduce the interference from the background.[39] Additionally, a few reported works have only focused on the detection of BSA but not on the associated interactions with BSA, which seem to have an effect on the quantification results. Even though it has been reported that squaraine dyes interact with BSA leading to fluorescent enrichment, no precise binding information relating to site I or site II has been attained.[40–42] To overcome these deficiencies, we have successfully synthesized a series of benzyl substituted berberine analogues (BZ_1–BZ_5) for interacting with and quantifying BSA.

In this manuscript, the center of attention is focused on benzyl substitution at the 9-*O*-position of berberine, an isoquinoline quaternary plant alkaloid for the sensing of BSA. In Scheme 1 we demonstrate the structures of the synthesized berberine analogues along with the different positions of chlorine (at the 2, 3, 4, and 2, 5 positions of the phenyl moiety) in order to control the two effects of hydrophobic interactions and steric repulsion. Among the derivatives, BZ_4 is exceedingly sensitive toward BSA and the emission intensity is amplified 140-fold upon the addition of a saturated concentration of BSA to the probe BZ_4 in CP buffer (10 mM, pH 7.2); a nanomolar detection value and strong eye-catching green fluorescence, observable *via* the naked eye, were obtained under a UV lamp at 365 nm. Selectivity experiments involving other proteins, like HSA, DNA, RNA, *etc.*, show this to be a superb selective BSA sensing probe. Another beauty of this work is that it includes a detailed investigation of the interactions of these synthesized analogues with BSA, and we fruitfully relate these results to the sensing outcomes.

2. Materials and methods

2.1 Instrumentation

^1H and ^{13}C NMR spectra of compounds BZ_2, BZ_3, and BZ_5 were recorded using a 600 MHz (or 150 MHz for ^{13}C) Bruker Lambda spectrometer, and for compounds BZ_1 and BZ_4, a Bruker AVANCE-III 500 MHz spectrometer was used at 25 °C, using TMS as an internal reference in DMSO-d_6 solvent. Mass data for compounds BZ_2, BZ_3, and BZ_5 were obtained using MALDI-ToF apparatus (VOYGER-DE PRO, Applied Biosystems, USA), and for compounds BZ_1 and BZ_4, a Bruker micro TOF QII high-resolution mass spectrometer was used. UV-vis spectra were acquired using a Shimadzu UV-1601 (Japan) spectrophotometer, and a PerkinElmer LS-55 (USA) spectrofluorimeter was used for fluorescence measurements with 2.5 nm excitation and 5 nm emission slit. Fluorescence lifetime experiments were performed using a DeltaFlex™ Modular fluorescence lifetime system (Horiba scientific, UK).

2.2 Reagents

Berberine chloride hydrate (BC), BSA (>98%), other proteins, nucleic acids, and enzymes were obtained from Sigma Aldrich (St. Louis, MO, USA). The other chemicals, like cationic salts, anionic salts, and all spectroscopic grade solvents, were acquired from Merck Pvt. Ltd. The chemicals were used without further purification, and solvents were distilled before use. Double distilled water was used for the preparation of citrate-phosphate (CP) buffer, containing 10 mM Na^+ at pH 7.2, and the berberine analogue, protein, enzyme, and nucleic acid solutions were prepared in CP buffer.

2.3 Synthesis of berberrubine (2)

Commercially available berberine chloride (**1**, 1000 mg) was heated to 190 °C in a vacuum oven under a reduced pressure of 20–30 mmHg for 15 min to get berberrubine (**2**, 885 mg) in 90% yield, according to a previously reported work.[43]

2.4 Synthesis of various benzyl substituted berberrubine derivatives (3a, 3b, 3c, 3d, 3e)

Various examples of benzyl chloride (1.5 mM) were added to solutions of **2** (1 mM) in CH_3CN in the presence of the base K_2CO_3 (1 mM); then the reaction mixtures were stirred for 4–6 h at 80 °C. The crude products were obtained upon evaporating the solvent under vacuum and washed with diethyl ether.

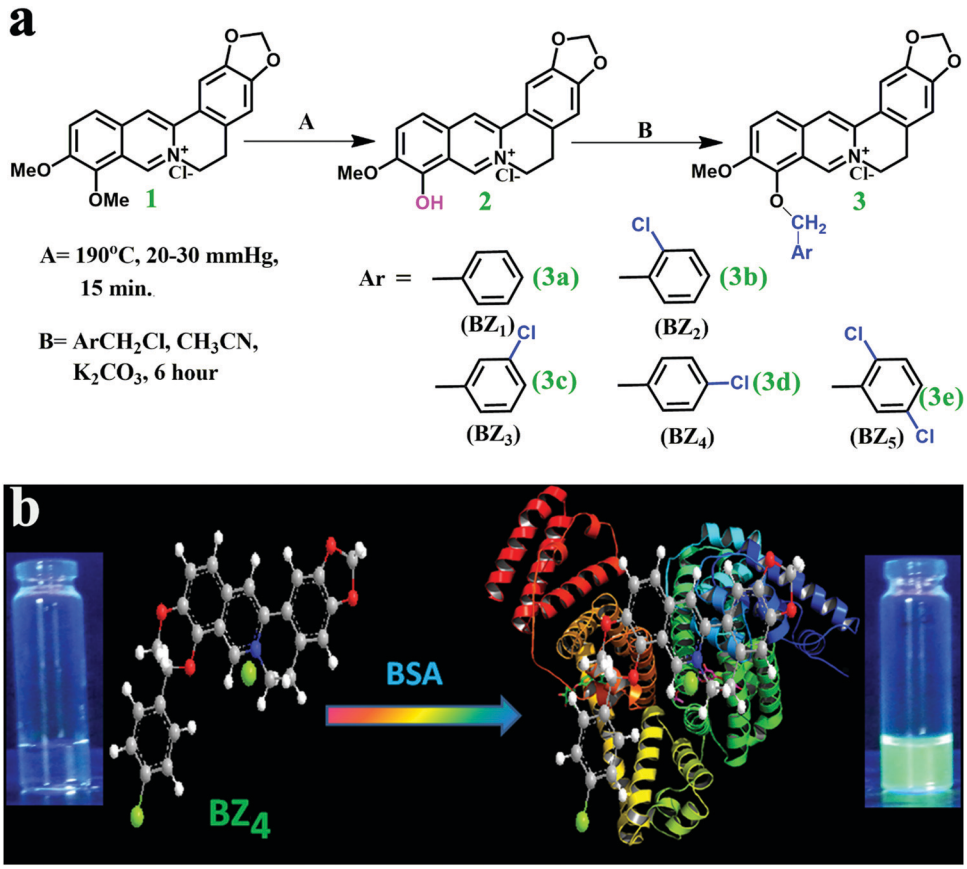

Scheme 1 (a) The synthetic route to the berberine analogues (BZ_1–BZ_5). (b) A schematic presentation of the BSA sensing mechanism adopted by the probe BZ_4.

The products were purified *via* column chromatography on a silica gel column and eluted with varying concentrations of a $CHCl_3$–CH_3OH solvent mixture to get the desired products (BZ_1–BZ_5). The berberine derivatives were well characterized using various methods, such as mass spectrometry, and ^1H, and ^{13}C NMR spectroscopies (Fig. S27–S41, ESI†).

2.5 The procedures for spectra measurements

2.5.1 Fluorescence measurements. Stock solutions of the probes (BZ_1–BZ_5), BSA, and other proteins, enzymes, and amino acids were prepared in CP buffer solution (10 mM, pH = 7.2). The fluorometric titration experiments were carried out using 1 mL of probe stock solution (5 μM) in a 1 cm path length quartz cell, and the various analytes stated above were gradually added from a micropipette to obtain the spectrum. For titration experiments, the excitation wavelength was fixed at 360 nm and the emission spectrum was gathered from 400 to 650 nm; the excitation and emission band widths were 5 nm and 5 nm, respectively. We also consider the inner filter effect during the gathering of fluorescence spectra *via* following equation

$$F_{corr} = F_{obs} \times e^{\frac{A_{exi}+A_{emi}}{2}} \quad (1)$$

where F_{corr} and F_{obs} signify the corrected and observed intensities, respectively, and A_{exi} and A_{emi} are the sums of protein and probe absorbance at the excitation and emission wavelengths, respectively.

2.5.2 Fluorescence quenching. During fluorescence quenching experiments, 295 nm was chosen as the excitation wavelength to discerningly excite the tryptophan moieties in proteins.[44] To nullify any contribution from the solvent to the fluorescence intensity, the background emission intensity of the blank buffer was deducted from every sample spectrum.

2.5.3 Absorbance measurements. UV-vis titration studies (interaction studies) of the probes were achieved using 1 mL of probe (5 μM) in 10 mM CP buffer at pH 7.2 in a 1 cm path length quartz cell over the range of 200 to 600 nm with increasing concentrations of BSA up to saturation.

2.5.4 IR-experiments. FTIR spectral studies were done to explore probe–BSA binding. Probe solution was gradually added to a protein solution under constant stirring to ensure the formation of a homogeneous solution and to achieve the two desired probe to BSA concentration ratios of 0.5 : 1 and 1 : 1. To ensure complex formation, spectra were collected after some time at room temperature with spectra gathered over the spectral range of 4000–600 cm^{-1} at a nominal resolution of 2 cm^{-1}.

2.5.5 Anisotropy measurements. Fluorescence polarization anisotropy measurements of probes at the BSA saturation concentration were made with the excitation wavelength and emission wavelength fixed at 360 and 531 nm, respectively.

The spectra were recorded after some time to ensure homogeneous complex formation and averages of five consecutive measurements are given.

2.6 Calculation of the detection limit

The detection limit of the probe BZ_4 for BSA detection was calculated based on fluorescence titration. To acquire the detection limit, BZ_4 (5 μM) was titrated with increasing concentrations of BSA (0–28 μM). The respective fluorescence intensity of BZ_4 was calculated 10 times without BSA, and the standard deviation of the blank measurements was obtained. To achieve the slope, the emission intensity at 517 nm was plotted against the concentration of BSA. Then, the detection limit was calculated using the equation: detection limit = $3.29\sigma/k$, where σ and k signify the standard deviation of the blank measurements and the slope of the I_{517} *vs.* concentration of BSA plot, respectively.

2.7 Fluorescence quantum yield calculations

The fluorescence quantum yields of the synthesized analogues (BZ_1–BZ_5) in the absence and presence of BSA were obtained using an optically comparable solution of quinine sulfate (Φ_r = 0.546 in 1 N H_2SO_4) as a standard (excitation wavelength of 365 nm). The quantum yield (Φ_s) is estimated using the given equation[45]

$$\Phi_s = \Phi_r \left(\frac{A_r F_s}{A_s F_r}\right)\left(\frac{\eta_s^2}{\eta_r^2}\right) \quad (2)$$

where A_r and A_s are, respectively, the absorbance of the reference and sample solutions, F_r and F_s signify the integrated emission intensities (areas) at the same excitation wavelength, and η represents the refractive index of the solvent.

2.8 Lifetime measurements

Lifetime decay data were assessed *via* the time-correlated single photon counting (TCSPC) method using CP buffer at pH 7.2 at an excitation wavelength of 372 nm from a laser LED source. The decay profile, $I(t)$, was calculated using the following equation[46]

$$I(t) = \sum_{i=1}^{\alpha} \alpha_i \exp\left(\frac{-t}{\tau_i}\right) \quad (3)$$

where α_i is the early emission intensity of the ith component having lifetime τ. The chi-square (χ^2) value specifies the best fitting parameter. The obtained data were scrutinized using EZ-time software. The mean lifetime (τ_m) of the sample under various experimental conditions was determined *via* the following equation

$$\tau_m = \frac{\sum_i \alpha_i \tau_i}{\sum_i \alpha_i} \quad (4)$$

2.9 Site marker experiments

To scrutinize the binding site of the analogue towards BSA, site marker displacement experiments were done using two site-specific markers, namely, warfarin, which specifically binds to Sudlow site I (sub-domain IIA), and ibuprofen, which specifically binds to Sudlow site II (sub-domain IIIA).[47] During performing this experiment, the site markers were increasingly added to a mixture of BZ_4 and BSA, while the other parameters, like excitation wavelength, and excitation and emission bandwidth, were identical to those used for the fluorescence titration experiments.

2.10 Docking studies

For close observations of changes in the microenvironment of BSA upon binding with BZ_4, we performed molecular docking studies. Accordingly, the three-dimensional (3D) structure of BZ_4 was drawn using MOE and energy optimized using the AM1 semi-empirical method with a RMS gradient of 0.001 kcal mol^{-1}.[48] The crystal structure of BSA (pdb id: 4f5s) was collected from the Protein Data Bank. Before docking, the binding sites were determined using site finder and 84 binding sites were found in BSA. The compound was docked to the best fitting domain of BSA, obtained *via* MOE, using the Alfa PMI placement method.

3. Result and discussion

3.1 UV-vis absorption study

Primarily, the absorption spectra of BZ_1–BZ_5 in the presence of bovine serum albumin were examined *via* UV-vis spectroscopy. The compound BZ_4 showed two absorption maxima at 423 nm and 345 nm in the wavelength region of 300–600 nm in CP buffer (10 mM, pH = 7.2). Upon the addition of BSA, the absorbance at 345 nm gradually decreased approaching saturation, with three clearly visible isosbestic points at 357, 364, and 373 nm (Fig. 1a). This result indicates the existence of interactions between the π electronic cloud of the probe and the tryptophan moiety in BSA,[49] and the notable hypochromic shift indicates that the probe is closer to BSA.[50] This may be attributed to the formation of a complex between the probe and BSA *via* electrostatic and hydrophobic interactions. Similarly, we performed the UV-vis titration of other probes with a gradual increase in the BSA concentration (Fig. S1, ESI†). Accordingly, the binding constant (K_{BH}) values for all probe (BZ_1–BZ_5)–BSA composites were evaluated from Benesi–Hildebrand plots (Fig. 1b), and data analysis was used to calculate a binding constant of 7.3×10^4 for the complex formed between BZ_4 and BSA (Table S1, ESI†).

3.2 Fluorescence titration experiments

Moreover, a strong indication of compound–BSA interaction comes from fluorescence spectral studies. All the compounds (BZ_1–BZ_5) were weakly fluorescent with insignificant fluorescence quantum yields upon excitation at their corresponding excitation wavelengths. Remarkable emission enhancement with a notable hypsochromic shift was observed upon the gradual addition of BSA up to saturation for all compound (BZ_1–BZ_5) solutions (Fig. S2, ESI†), and the comparatively highest emission intensity increase (~140 fold) was noticed in the

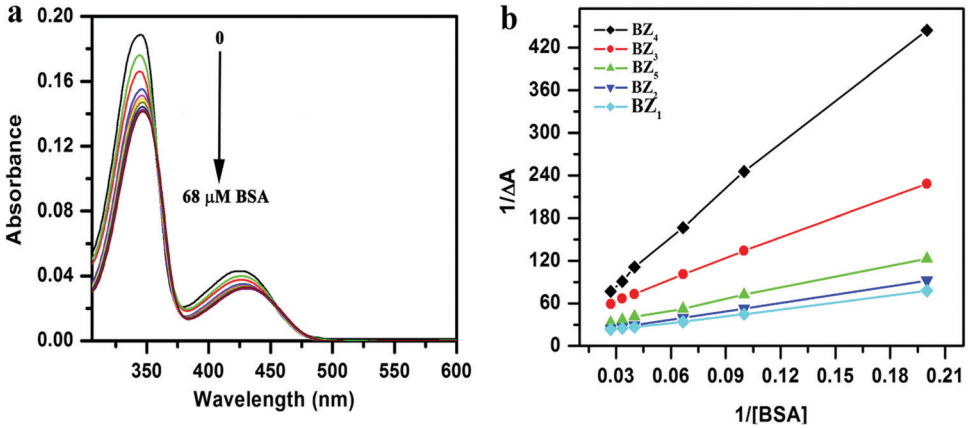

Fig. 1 (a) UV-vis spectra of BZ_4 (5 μM) with an increasing concentration of BSA, ranging from 0–68 μM, in CP buffer (pH 7.2, 10 mM). (b) Benesi–Hildebrand plots of all synthesized analogues (BZ_1–BZ_5) upon the addition of varying concentrations of BSA.

case of probe BZ_4. This drastic change in the fluorescence signal could offer the potential for ocular BSA sensing, as depicted in Scheme 1. Plots of the emission intensities of the probes against BSA concentration (Fig. S3, ESI†) demonstrated that the probe BZ_4 showed a good linear relationship compared to the other compounds (Table S2, ESI†) and the fluorescence quantum yield (Φ) after binding with BSA was highest for compound BZ_4 (Table 1). Therefore, all the above factors led us to speculate that the derivative BZ_4 (3d) had the highest sensitivity towards BSA (Fig. 2a) and in this manuscript, we used the analogue BZ_4 for the quantification of BSA during *in vitro* analysis. The linearity range for BSA sensing using probe BZ_4 extended up to 2.5 μM (Fig. 2b) and the detection limit according to IUPAC conventions ($3.29\sigma/K$) was found to be 3.3 nM, making this a superior BSA detection probe. The differences in the BSA sensing capabilities of these compounds ($BZ_4 > BZ_3 > BZ_5 > BZ_2 > BZ_1$) are rationalized based on the different positions of the chlorine group in the benzyl substituent. We argue that competition between two factors, namely hydrophobic interactions and steric repulsion, is responsible for the sensing abilities of the probes. When Cl is situated at the 4-position, minimum steric repulsion exists; however, maximum hydrophobicity provokes compound BZ_4 to efficiently interact with BSA. Steric repulsion increases and hydrophobicity decreases for the 3-chlorobenzyl, 2,5-dichlorobenzyl and 2-chlorobenzyl substituents in respective order.

Table 1 The photophysical properties of the berberine analogues[a] in the absence and presence of BSA at 25 °C

Entry	Φ^b	$\tau_m{}^c$ (ns)	$k_{nr} \times 10^8$ (s^{-1})	r^d	$K_a \times 10^4$ (M^{-1})
BZ_1	4.2×10^{-3}	0.98	10.16	0.1126	—
BZ_2	6.4×10^{-3}	0.95	10.45	0.1129	—
BZ_3	5.2×10^{-3}	0.93	10.69	0.1128	—
BZ_4	4.0×10^{-3}	0.68	14.64	0.113	—
BZ_5	5.3×10^{-3}	1.81	5.4	0.1127	—
BZ_1 + BSA	0.032	6.28	1.54	0.1149	2.2×10^4
BZ_2 + BSA	0.042	5.22	1.83	0.1163	3.1×10^4
BZ_3 + BSA	0.104	6.46	1.38	0.1195	5.2×10^4
BZ_4 + BSA	0.17	9.20	0.90	0.12337	5.6×10^4
BZ_5 + BSA	0.08	6.56	1.40	0.1188	4.3×10^4

[a] 5 μM analogue. [b] Quantum yield with respect to quinine sulfate. [c] Average lifetime. [d] Anisotropy.

3.3 Selectivity and sensitivity

The naked eye visualization under a UV lamp of all these probe solutions (5 μM) upon the addition of BSA and HSA (28 μM) revealed that BZ_4 was a superb selective probe for BSA (Fig. 3a). The fluorescence intensity, as well as the emission maximum, is almost the same upon the addition of various analytes, such as different cationic and anionic salts (28 μM), to the probe (BZ_4) solution (Fig. S4–S7, ESI†). Interestingly, upon the addition of other proteins or enzymes, like hemoglobin, ribonuclease A, insulin, tryptophan, trypsin, *etc.*, the emission signal was not significantly altered; however, in the presence of DNA and RNA, the fluorescence intensity was somewhat increased (Fig. 3b and c). We have already discussed that hydrophobic interactions are the foremost factor responsible for BSA sensing and, accordingly, selectivity studies reflect that other proteins and enzymes do not have appropriate hydrophobic regions to bind with the probe.[51] The hydrophobicity of these proteins depends on various factors, like the amino acid sequences, protein structures, and side chains, and BSA is assumed to have higher hydrophobicity than the other proteins/enzymes used. However, berberine, a DNA/RNA interacting plant alkaloid, and, similarly, the synthesized berberine analogues also interact with DNA/RNA; therefore, the emission intensity increased a little but not significantly compared to the addition of BSA. Competitive experiments, *i.e.*, studying the emission intensity of BZ_4 upon the addition of BSA in the presence of other proteins or enzymes, indicate that the presence of these proteins/enzymes was insignificant to hamper the detection of BSA (Fig. 3b).

3.4 Binding stoichiometry (Job's plot)

To determine the binding stoichiometry between the probe BZ_4 and BSA, we obtained a Job's plot, where the concentration of the both probe and BSA remain fixed, but the mole fraction of both is altered. Here, we plot the fluorescence intensity of the solution, keeping a fixed concentration (5 μM) of probe and BSA

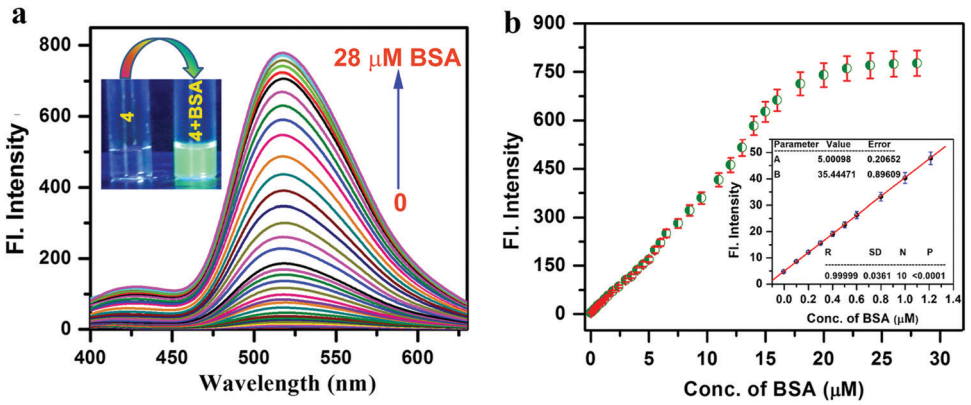

Fig. 2 (a) The emission spectra of BZ_4 (5 μM) upon the addition of increasing concentrations of BSA (0–28 μM) in CP buffer (pH 7.2 and 10 mM). (b) The fluorescence intensity at 517 nm of probe BZ_4 (5 μM), which was linearly related to the concentration of BSA (0–2.5 μM) in CP buffer (pH 7.2, 10 mM); λ_{ex} = 360 nm.

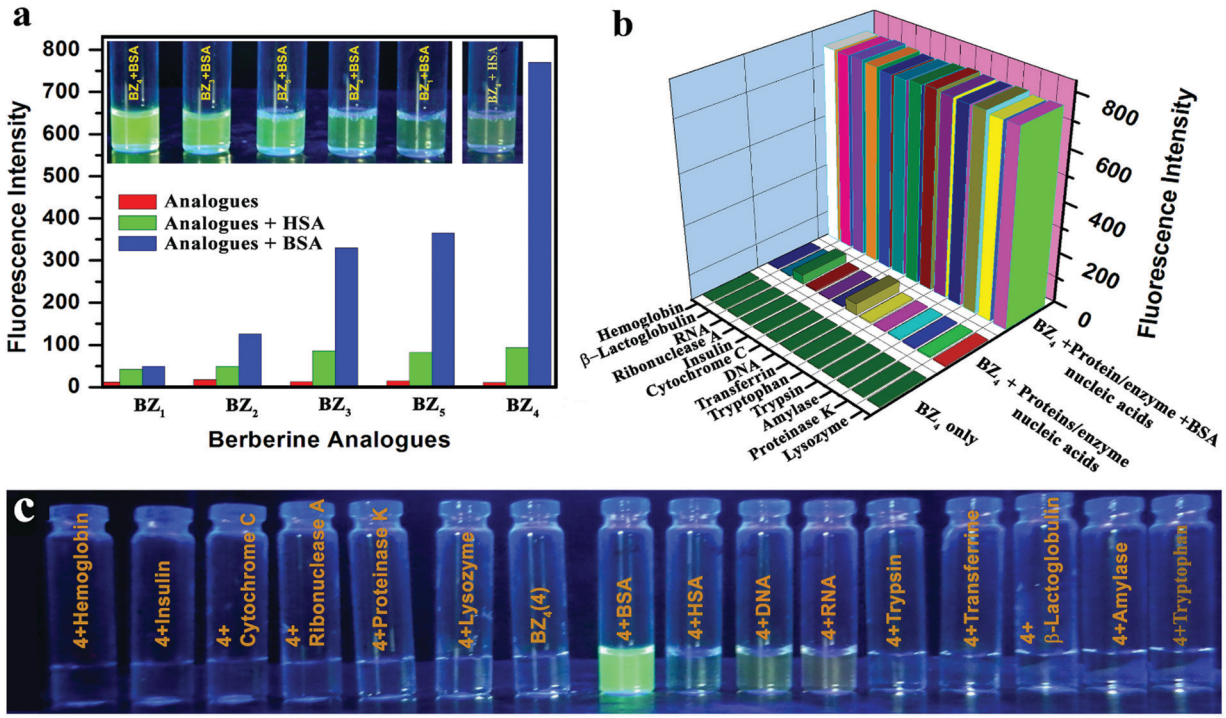

Fig. 3 (a) The fluorescence intensities of the synthesized analogues (5 μM) upon the addition of 28 μM HSA/BSA; corresponding optical images under UV light at 365 nm are depicted in the inset. (b) The fluorescence responses of probe BZ_4 (5 μM) to other biological interferents, (DNA, RNA, ribonuclease A, insulin, cytochrome *C*, β-lactoglobulin, lysozyme, hemoglobin, proteinase K, trypsin, tryptophan, transferrin, amylase; 28 μM) in CP buffer (pH 7.2, 10 mM), λ_{ex} = 360 nm. (c) Optical photos of BZ_4 probe solution upon the addition of various proteins/enzymes/amino acids under a UV lamp at 365 nm.

while varying the mole fraction; the fit lines intersected nicely at a binding stoichiometry of 1 : 1 (Fig. S8, ESI†). These results further clarified that the analogue molecule bound to one binding site of BSA.

3.5 Site-selective binding

Site marker experiments were carried out to gain insight into the probe–BSA interactions. For this experiment, warfarin and ibuprofen were chosen as site I and site II markers, respectively. The abrupt decrease in emission intensity upon the introduction of ibuprofen to the BZ_4–BSA complex indicates that probe BZ_4 was replaced by ibuprofen from the protein microenvironment. Overall, 65% replacement and 25% replacement of BZ_4 were realized upon the addition of ibuprofen and warfarin to the BZ_4–BSA complex, respectively (Fig. 4a and Fig. S9, S10, ESI†). The results indicate that probe BZ_4 has stronger binding affinity towards site II than site I. The greater binding affinity of BZ_4 for site II was predominantly due to a combination of electrostatic and hydrophobic interactions.[44]

3.6 Fluorescence anisotropy

The fluorescence anisotropy indicates the rigidity of a fluorophore microenvironment and provides additional evidence in favor of interactions between the probes and BSA. An enhancement in the fluorescence anisotropy reflects greater rigidity in the surrounding fluorophore environment. Plots of the fluorescence anisotropy (r) of the compounds against the concentration of added BSA show that upon increasing the BSA concentration, the anisotropy increases for all analogues (Fig. 4b), and the respective r values are depicted in Table 1. The greater increase in the anisotropy in the case of probe BZ_4 compared to the other examples suggests that the restricted of rotation is maximum upon the introduction of BSA and, furthermore, that probe BZ_4 is more strongly bound with BSA compared to the other probes.

3.7 Effects of pH on the probe–BSA complex

Changes in the fluorescence intensity during probe BZ_4–BSA complex formation at various pH levels could also occur if our probe is applied in biological systems. The fluorescence intensity of the BZ_4–BSA complex in the physiological pH range, acidic pH range, and basic pH range were investigated and the probe showed maximum emission intensity enhancement in the presence of a BSA microenvironment at physiological pH (Fig. S11, ESI†). We chose a physiological pH value of 7.2 for the experiments in this article.

3.8 The fluorescence lifetimes of analogues in the presence of BSA

Fluorescence lifetime measurements enhance our knowledge about the microenvironment in the region of a fluorophore and can be used to explore excited state interaction phenomena.[3] Accordingly, we performed time-correlated single photon counting (TCSPC) experiments on all analogues in the absence and presence of BSA. The TCSPC (lifetime) data of BZ_4 (Fig. 5b) demonstrated that in the absence of BSA, tri-exponential decay was exhibited with a mean lifetime (τ_m) of 0.83 ns; in the presence of BSA, the tri-exponential decay significantly increased with a mean lifetime (τ_m) of 6.12 ns (Table 2). The non-radiative decay constant (k_{nr}) values of BZ_4, with the help of lifetime and fluorescence quantum yield data, were established as 14.64×10^8 and 0.90×10^8 s^{-1} in the absence and presence of BSA, respectively, which suggests that migration from an aqueous to a protein environment decreased the k_{nr} values. Thus, the decrease in the non-radiative rate in the presence of BSA tunes the lifetime enhancement of BZ_4 in the protein environment, and the results reveal that probe BZ_4 strongly binds to BSA *via* hydrophobic interactions. We also performed the above-mentioned experiments on the other compounds (Fig. S12, ESI†), and it was observed that the lifetime enhancement is highest in the case of BZ_4 in the presence of BSA (Table 2), which strongly corroborates our previous experiments.

3.9 Fluorescence lifetime decay of BSA in the presence of the analogues

Fluorescence lifetime measurements also enhance our knowledge of the interactions between probes and proteins;[44] accordingly, we perform time-correlated lifetime experiments involving BSA in the absence and presence of the analogues. The best-fit decay profile of native BSA exhibited a triexponential function, where the corresponding lifetimes are 2.03, 4.79, and 7.66 ns, and the average lifetime is 5.86 ns, in good concurrence with the literature value.[41] Upon the successive addition of the analogues (BZ_1–BZ_5) to BSA solution, the mean lifetime values of BSA showed few changes, as shown in Fig. S13 and in Table S4 (ESI†). The results signify the formation of complexes between BSA and the analogues, followed by the alteration of the microenvironment around BSA. The insignificant changes in the lifetime values indicate that the fluorescence quenching process is static in nature, which is mainly due to ground state complex formation between the protein and berberine analogues.

3.10 Proposed sensing mechanism

Taking together all of the above experimental findings, such as absorption titration, fluorescence titration, fluorescence quenching and lifetime measurements, it is indicated that the positional difference of the Cl atom affects the interactions between the synthesized probe molecules (BZ_1–BZ_5) and BSA;

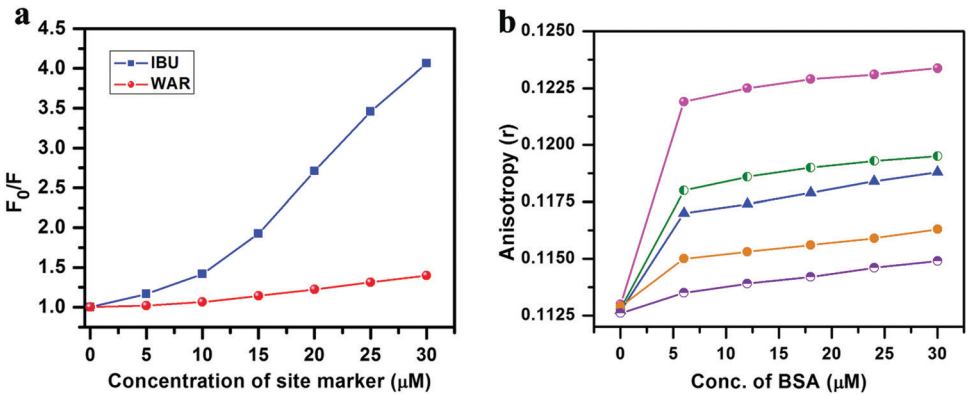

Fig. 4 (a) Site marker experiments: plots of F_0/F for BZ_4 + BSA complexes upon the addition of two site markers, namely warfarin and ibuprofen. (b) The variation of the fluorescence anisotropy (r) of the probes (5 μM) upon the addition of various concentration of BSA at an emission wavelength of 517 nm (pink: BZ_4; green: BZ_3; blue: BZ_5; orange: BZ_2; purple: BZ_1).

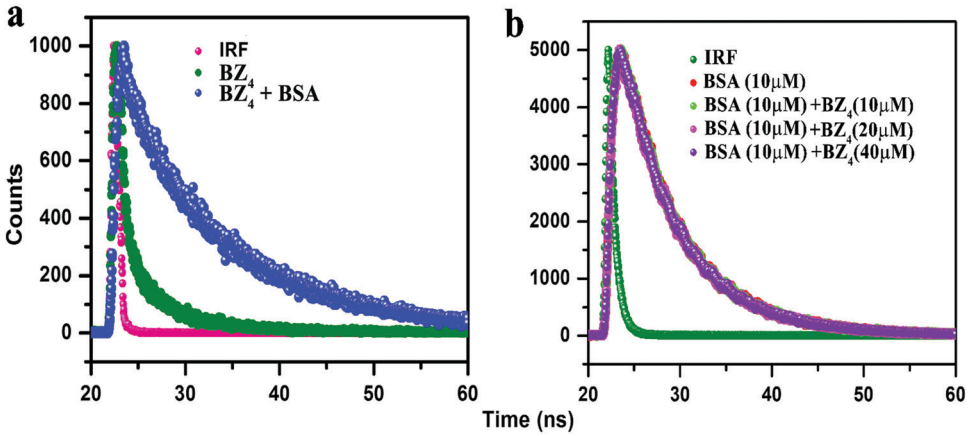

Fig. 5 (a) TCSPC spectra of BZ_4 (5 μM) in the absence and presence of BSA (28 μM) in CP buffer (pH 7.0, 10 mM Na^+). (b) TCSPC spectra of BSA in the presence of different concentrations of probe BZ_4 in CP buffer (pH 7.0, 10 mM Na^+).

Table 2 Lifetime data from the berberine analogues in the absence and presence of BSA

Entry	τ_1 (ns)	α_1	τ_2 (ns)	α_2	τ_3 (ns)	α_3	τ_m (ns)	χ^2
BZ_1	0.27	0.82	2.05	0.10	6.99	0.08	0.98	1.06
BZ_1 + BSA	0.60	0.25	3.71	0.32	11.5	0.43	6.28	1.03
BZ_2	0.25	0.81	1.73	0.11	7.02	0.08	0.95	1.07
BZ_2 + BSA	0.74	0.38	3.74	0.29	11.7	0.33	5.22	1.08
BZ_3	0.30	0.82	2.1	0.10	6.72	0.07	0.93	1.09
BZ_3 + BSA	0.67	0.28	3.79	0.26	11.5	0.46	6.46	1.05
BZ_4	0.24	0.83	1.36	0.10	5.01	0.07	0.68	1.03
BZ_4 + BSA	1.13	0.20	5.97	0.21	13.1	0.59	9.20	1.05
BZ_5	0.35	0.74	2.26	0.14	7.32	0.17	1.81	1.01
BZ_5 + BSA	0.64	0.27	3.71	0.28	11.9	0.45	6.56	1.09

consequently, the sensing abilities of these probes are affected. Furthermore, a control experiment involving the addition of BSA to berberine solution resulted in no significant alterations to the fluorescence spectrum, while the addition of BSA to a benzyl group-containing berberine analogue resulted in lesser changes to the spectra. The above-mentioned control experiments further indicate the effects of the position of the Cl atom in the benzyl moiety. The above-mentioned experiments reflect that the order of binding affinity of the probes was $BZ_4 > BZ_3 > BZ_5 > BZ_2 > BZ_1$, and the fluorescence titration studies revealed that sensing ability for BSA of these probes was in the order $BZ_4 > BZ_3 > BZ_5 > BZ_2 > BZ_1$. Thus, we assume that competition between two factors, *i.e.*, hydrophobic interactions and steric repulsion, is accountable for the sensing capabilities of the probes. When Cl is situated at the 4-position, minimum steric repulsion and maximum hydrophobicity tunes the compound, BZ_4, to efficiently interact with BSA; however, steric repulsion increases and hydrophobicity gradually decreases for the 3-chlorobenzyl, 2,5-dichlorobenzyl and 2-chlorobenzyl substituents. To gain insight into the interactions between the compounds and BSA, it is necessary to inspect the interactions between the free amino acid tryptophan and BZ_4. Consequently, we performed a control experiment involving the addition of tryptophan to BZ_4 solution and no noteworthy spectral changes were observed (Fig. S14, ESI†); this points out the fact that the microenvironment around the tryptophan moiety in BSA provokes the drastic spectral changes upon the introduction of BSA to probe solution.

3.11 Three-dimensional fluorescence spectral studies

3D fluorescence spectroscopy was carried out by concurrently changing the excitation and emission wavelengths, reflecting changes in the microenvironment of the protein upon interaction with the compounds (BZ_1–BZ_5).[52] The 3D spectra of BSA in the absence and presence of the compounds are presented in Fig. S15–S20 (ESI†) and the results are listed in Table S5 (ESI†). The spectra demonstrate four distinct peaks: peak "a" signifies first-order Rayleigh scattering ($\lambda_{em} = \lambda_{ex}$), and peak "b" is the second-order Rayleigh scattering peak ($\lambda_{em} = 2\lambda_{ex}$). Peak 1 ($\lambda_{ex}$ = 280 nm, λ_{em} = 345 nm) is due to the characteristic spectra of both Tyr and Trp as BSA was excited at 280 nm, and peak 2 (λ_{ex} = 230 nm, λ_{em} = 345 nm) is due to the fluorescence spectrum of the polypeptide backbone in BSA. In the case of peak 1, there was a considerable Stokes shift with a decrease in the fluorescence intensity; in the case of peak 2, there was also a decrease in the fluorescence intensity, and significant Stokes shifts were observed in the order $BZ_4 > BZ_3 > BZ_5 > BZ_2 > BZ_1$. This type of Stokes shift indicates that the polarity of both components (Trp and Tyr) decreased and BSA was suppressed into a hydrophobic pocket (Table S5, ESI†). The decreases in the emission intensities of peaks 1 and 2 indicate the occurrence of interactions between the probes and BSA, leading to changes in the microenvironment around Trp along with the structural alteration of BSA.

3.12 Fluorescence quenching studies

The quenching of the fluorescence of a protein upon binding with a ligand offers significant information about changes in the microenvironment of the protein in close proximity with the ligand molecule. The fluorescence properties of BSA are predominantly due to the presence of two tryptophan moieties,

namely Trp-134 and Trp-212, in the I and II domains, respectively. The emission spectrum of BSA exhibits an enhanced fluorescence signal at 345 nm upon excitation at 295 nm in buffer solution, and it should be noted that we selectively chose an excitation wavelength of 295 nm rather than 280 nm to minimize the fluorescence contribution from the tyrosine moiety present in BSA. The fluorescence spectrum of BSA was remarkably changed upon the addition of different concentrations of probes. Fig. 6a shows that the steady state fluorescence intensity of BSA decreased gradually upon the successive introduction of BZ_4 up to saturation, with a large red shift of 27 nm. Also, the fluorescence intensity of BSA decreased up to saturation accompanied by a red shift upon the addition of the other probes (Fig. S20 and S21, ESI†). This type of spectral change, a red shift with a decrease in the emission intensity, indicates a strong interaction between the probe and BSA, and the microenvironment of tryptophan may change from hydrophobic or less hydrophilic to a hydrophilic environment. The maximum decrease in the fluorescence intensity of BSA and the larger red shift upon the addition of BZ_4 indicate its strong interaction with BSA compared to the other probes. Consequently, we calculate the quenching constant by applying the Stern–Volmer equation in the form

$$\frac{F_0}{F} = 1 + K_q\tau_0[\mathrm{Q}] = 1 + K_{\mathrm{SV}}[\mathrm{Q}] \quad (5)$$

where F_0 and F represent the fluorescence intensities of BSA in the absence and presence of the quencher, respectively, [Q] indicates the concentration of quencher, and K_{SV} is the Stern–Volmer quenching constant. Stern–Volmer plots of F_0/F against the probe concentration for all probes are depicted in Fig. S21 and S22 (ESI†) and each plot is linear in nature; the K_{SV} values for each probe are shown in Table S6 (ESI†). We can also calculate the probe–BSA binding constant (K_A) values and number of binding sites (n) from quenching experiments (Fig. 6b), assuming that BSA has the same independent binding sites, using the following equation

$$\log\frac{F_0 - F}{F} = \log K_{\mathrm{A}} + \log[\mathrm{Q}] \quad (6)$$

where F_0, F, and [Q] denote the terms stated above; the obtained binding constant and n values are listed in Table S6 (ESI†). The binding constant value of the BZ_4–BSA complex was found to be higher than those of the other probe–BSA complexes, indicating greater quenching efficiency, and the n values for all the probe–BSA complexes were almost one, indicating that the probes are situated at one binding site.

3.13 Binding study *via* FT-IR

Further conformation regarding berberine analogue–BSA complexation comes through FT-IR spectral analysis. The changes in the intensities at 1656 cm^{-1} (amide I band), a mainly C═O stretching mode, and at 1543 cm^{-1} (amide II band), C–N stretching coupled with N–H bending modes of native BSA, were monitored upon the addition of the analogues.[52] Also, IR derivative plot and curve fitting methods were applied to investigate changes in the secondary structure of the protein upon the addition of the analogues. The intensities of the stretching frequencies at 1653 and 1546 cm^{-1} decreased gradually with an increase in the concentration of the analogue BZ_4 (Fig. 7a). The decrease in the intensities of the amide I and II bands signifies a decrease in the α-helix content of BSA upon the addition of analogue BZ_4. The IR-derivative plot is shown in Fig. 7b, and the corresponding results are given in Table S8 (ESI†), which also indicate a reduction in α-helix content upon BSA–BZ_4 complexation. Similarly, IR spectral analyses of BSA in the presence of the other analogues are given in the ESI† (Fig. S23–S26).

3.14 Molecular docking studies

The molecular docking of BZ_4 with BSA was performed to gain insight into changes in the protein microenvironment and provide further confirmation about site-specific binding during BZ_4–BSA binding. As a previous experiment (the site marker study) concluded that the probe (BZ_4) bound to sub-domain IIIA (the ibuprofen binding site), we positioned BZ_4 at the sites of this domain. The lowest MOE energy outcome (Table S8, ESI†) specified that the ligand bound to sub-domain IIIA better

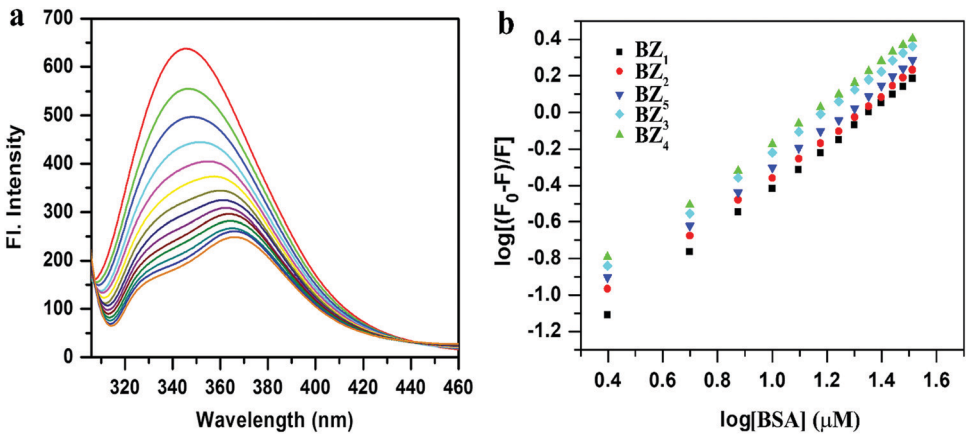

Fig. 6 (a) Fluorescence spectra of 5 μM BSA in the presence of increasing concentrations of probe BZ_1 (0 to 40 μM) at pH 7.2 in 10 mM CP buffer. (b) Modified Stern–Volmer plots of $\log[(F_0 - F)/F]$ *vs.* log[BSA] for all BSA–probe complexes at pH 7.2.

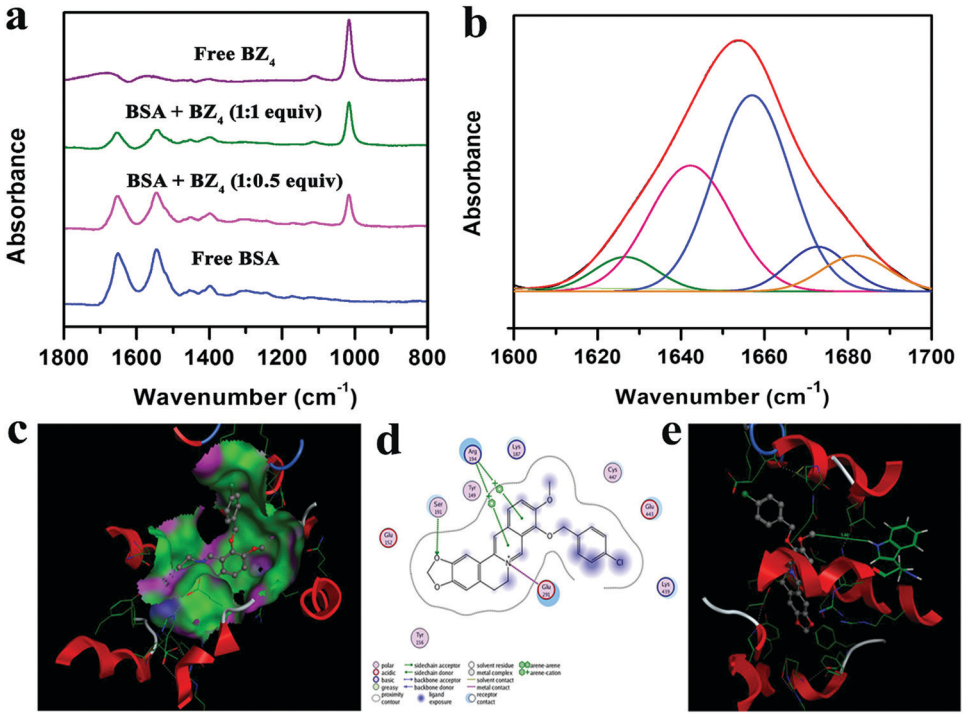

Fig. 7 (a) FT-IR spectra in the region of 1800 to 800 cm^{-1} from hydrated films (pH 7.2, 10 mM Na^+ CP buffer, 25 °C) of free BSA and its complexes (BSA + BZ_4) at different concentrations. (b) Second derivative resolution enhancement and the curve-fitted amide I region (1700–1600 cm^{-1}). (c) A 3D binding picture of BZ_4 when docked with BSA. (d) A 2D representation of the conformation of BZ_4 when docked with BSA. (e) The binding distance between BZ_4 and tryptophan (Trp) 212 of BSA.

than the other sites. This result indicates that the ligand interacts with BSA at the hydrophobic cavity of sub-domain IIIA of BSA (Fig. 7c). The analogue was surrounded by hydrophobic and negatively charged residues, such as Arg194, Tyr 149, Ser 191, Glu 152, and Glu 191. From Fig. 7d, it is clear that a hydrogen bond between Ser 191 and an oxygen atom of the analogue stabilizes the complex. Besides, an arene-cation interaction between Arg 194 and the analogue aromatic ring also played a vital role in complex formation. The positive charge of the nitrogen present in the ligand was also an important factor. From the arrangement of the analogue, it was observed that most of the analogue penetrates into the binding pocket of BSA, suggesting that the binding was mainly hydrophobic in nature. The distance between the Trp 212 residue and the ligand was about 5.66 Å (Fig. 7e), and the free energy was −9.34 kcal mol^{-1}, which further affirms the obtained experimental results.

4. Conclusions

In summary, we have synthesized a new series of berberine analogues *via* the different positioning of a chlorobenzyl molecule at the 9-*O* position of the mother berberine, and the protein binding and structure-optical sensing properties of these analogues towards BSA detection were investigated in depth. The investigation revealed that the analogues interact with BSA non-covalently and cause an increase in the emission intensity. The superiority of this study lies in the huge increase in the emission intensity (140-fold) as well as the quantum yield (43 fold) of BZ_4 upon the addition of BSA, while changes in the emission signal upon the addition of various other proteins/enzymes are insignificant under a similar set of investigation conditions; this heralds a potential new, hydrophobic, turn-on fluorescence sensor (BZ_4) for the selective and nanomolar quantification of BSA. Dye displacement experiments and molecular docking simulations revealed that probe BZ_4 has strong binding affinity towards site II of BSA. Experimental tools like absorption titration, fluorescence titration, fluorescence quenching, fluorescence anisotropy and lifetime measurements showed that the microenvironment produced by bovine serum albumin and the structural restriction of the probe, involving steric, H-bonding and electronic factors, is the decisive factor determining the fluorescence signaling of BSA, and we usefully showed how two factors, namely steric effects and the hydrophobicity of these analogues, affect the detection of BSA. From the above results, we suppose that this work definitely provides an idea for designing plant alkaloid-based probes for SA in the future, and we strongly deem that these BSA selective probes will have great impact in future biomedical research.

Conflicts of interest

There are no conflicts to declare.

Acknowledgements

Sk. Nayim and Mt. Nasima Aktara acknowledge the UGC for MANF fellowships and Somnath Das also acknowledges the

UGC for a junior research fellowship. We are also thankful to UGC-SAP DRS-II and DST-FIST New Delhi and USIC for providing instrument facilities.

References

1 R. Kubota and I. Hamachi, *Chem. Soc. Rev.*, 2015, **44**, 4454.
2 (*a*) Y. Xu, Q. Liu, X. Li, C. Wesdemiotisa and Y. Pang, *Chem. Commun.*, 2012, **48**, 11313; (*b*) P. Zhang, Y. Xiao, Q. Zhang, Z. Zhang, H. Yu and C. Ding, *New J. Chem.*, 2019, **43**, 7620.
3 (*a*) G. Dey, P. Gaur, R. Giri and S. Ghosh, *Chem. Commun.*, 2016, **52**, 1887; (*b*) P. Zhang, Q. Zhang, S. Li, W. Chen, X. Guo and C. Ding, *J. Mater. Chem. B*, 2019, **7**, 1238; (*c*) P. Zhang, X. Guo, Y. Xiao, Q. Zhang and C. Ding, *Spectrochim. Acta, Part A*, 2019, **223**, 117318.
4 A. Chakrabarty, A. Mallick, B. Haldar, P. Das and N. Chattopadhyay, *Biomacromolecules*, 2007, **83**, 920.
5 J. Rozga, T. Piatek and P. Małkowski, *Ann. Transplant.*, 2012, **18**, 205.
6 J. P. Doweiko and D. J. Nompleggi, *J. Parenter. Enteral Nutr.*, 1991, **15**, 207.
7 M. Fasano, S. Curry, E. Terreno, M. Galliano, G. Fanali, P. Narciso, S. Notari and P. Ascenzi, *IUBMB Life*, 2005, **57**, 787.
8 M. Dockal, D. C. Carter and F. Ruker, *J. Biol. Chem.*, 1999, **274**, 29303.
9 R. Dolhofer and O. H. Wieland, *Diabetes*, 1980, **29**, 417.
10 R. R. Anderson, R. L. Holliday, A. A. Driedger, M. Lefcoe, B. Reid and W. Sibbald, *Am. Rev. Respir. Dis.*, 1979, **119**, 869.
11 C. E. Guthrow, M. A. Morris, J. F. Day, S. R. Thorpe and J. W. Baynes, *Proc. Natl. Acad. Sci. U. S. A.*, 1979, **76**, 4258.
12 V. Arroyo, *Aliment. Pharmacol. Ther.*, 2002, **16**, 1.
13 H. Sugimori, F. Tomoda, T. Koike, H. Kurosaki, T. Masutani, M. Ohara, S. Kagitani and H. Inoue, *Hypertens. Res.*, 2013, **36**, 247.
14 M. C. Corti, J. M. Guralnik, M. E. Salive and J. D. Sorkin, *J. Am. Med. Assoc.*, 1994, **272**, 1036.
15 D. D. Zeeuw, H. H. Parving and R. H. Henning, *J. Am. Soc. Nephrol.*, 2006, **17**, 2100.
16 G. J. Quinlan, G. S. Martin and T. W. Evans, *Hepatology*, 2005, **41**, 1211.
17 X. M. He and D. C. Carter, *Nature*, 1992, **358**, 209–215.
18 V. Lhiaubet-Vallet, Z. Sarabia, F. Bosca and M. A. Miranda, *J. Am. Chem. Soc.*, 2004, **126**, 9538.
19 M. C. Jimenez, M. A. Miranda and I. Vaya, *J. Am. Chem. Soc.*, 2005, **127**, 10134.
20 K. Szacilowski, W. Macyk, A. Drzewiecka-Matuszek, M. Brindell and G. Stochel, *Chem. Rev.*, 2005, **105**, 2647.
21 R. K. Pandey, S. Constantine, T. Tsuchida, G. Zheng, C. J. Medforth, M. Aoudia, A. N. Kozyrev, M. A. J. Rodgers, H. Kato, K. M. Smith and T. J. Dougherty, *J. Med. Chem.*, 1997, **40**, 2770.
22 K. Pinwattana, J. Wang, C. T. Lin, H. Wu, D. Du, Y. Lin and O. Chailapakul, *Biosens. Bioelectron.*, 2010, **26**, 1109.
23 B. T. Doumas, W. A. Watson and H. G. Biggs, *Clin. Chim. Acta*, 1997, **258**, 21.
24 M.-C. Tu, Y.-T. Chang, Y.-T. Kang, H.-Y. Chang, P. Chang and T.-R. Yew, *Biosens. Bioelectron.*, 2012, **34**, 286.
25 Y. H. Chuang, Y. T. Chang, K. L. Liu, H. Y. Chang and T. R. Yew, *Biosens. Bioelectron.*, 2011, **28**, 368.
26 M. Kukkar, A. Sharma, P. Kumar, K. H. Kim and A. Deep, *Anal. Chim. Acta*, 2016, **939**, 101.
27 Z. H. Lin, I. C. Chen and H. T. Chang, *Chem. Commun.*, 2011, **47**, 7116.
28 X. Xu, J. Huang, J. Li, J. Yan, J. Qin and Z. Li, *Chem. Commun.*, 2011, **47**, 12385.
29 X. Fan, Q. He, S. Sun, H. Li, Y. Pei and Y. Xu, *Chem. Commun.*, 2016, **52**, 1178.
30 L. Wang, L. Yang, L. Zhu, D. Cao and L. Li, *Sens. Actuators, B*, 2016, **231**, 733.
31 C. Liu, W. Yang, Q. Gao, J. Du, H. Luo, Y. Liu and C. Yang, *J. Lumin.*, 2018, **197**, 193.
32 Y. Xu, Q. Liu, X. Li, C. Wesdemiotis and Y. Pang, *Chem. Commun.*, 2012, **48**, 11313.
33 H. Sunahara, Y. Urano, H. Kojima and T. Nagano, *J. Am. Chem. Soc.*, 2007, **129**, 5597.
34 C. A. Haskard and E. C. Y. Li-Chan, *J. Agric. Food Chem.*, 1998, **46**, 2671.
35 N. Alizadeh-Pasdar and E. C. Y. Li-Chan, *J. Agric. Food Chem.*, 2000, **48**, 328.
36 S. J. Kim, H. W. Rhee, H. J. Park, H. Y. Kim, H. S. Kim and J. I. Hong, *Bioorg. Med. Chem. Lett.*, 2013, **23**, 2093.
37 J. Kumpf, J. Freudenberg and U. H. F. Bunz, *Analyst*, 2015, **140**, 3136–3142.
38 Y. Wang, Y. Zhong, Q. Wang, X. F. Yang, Z. Li and H. Li, *Anal. Chem.*, 2016, **88**, 10237–10244.
39 B. Liu, Y. Pang, R. Bouhenni, E. Duah, S. Paruchuri and L. McDonald, *Chem. Commun.*, 2015, **51**, 11060–11063.
40 V. S. Jisha, K. T. Arun, M. Hariharan and D. Ramaiah, *J. Phys. Chem. B*, 2010, **114**, 5912.
41 Y. Xu, Z. Li, A. Malkovskiy, S. Sun and Y. Pang, *J. Phys. Chem. B*, 2010, **114**, 8574.
42 B. Wang, J. Fan, S. Sun, L. Wang, B. Song and X. Peng, *Dyes Pigm.*, 2010, **85**, 43.
43 G. C. Jana, M. Khatun, Sk. Nayim, S. Das, A. Maji, M. Beg, A. Patra, P. Bhattacharjee, K. Bhadra and M. Hossain, *New J. Chem.*, 2019, **43**, 2368.
44 B. Ojha and G. Das, *Chem. Commun.*, 2010, **46**, 2079.
45 A. M. Brouwer, *Pure Appl. Chem.*, 2011, **83**, 2213.
46 R. Swaminathan, G. Krishnamoorthy and N. Periasamy, *Biophys. J.*, 1994, **67**, 2013.
47 S.-F. Ma, M. Anraku, Y. Iwao, K. Yamasaki, U. Kragh-Hansen, N. Yamaotsu, S. Hirono, T. Ikeda and M. Otagiri, *Drug Metab. Dispos.*, 2005, **33**, 1911.
48 H. Hamishehkar, S. Hosseini, A. Naseri, A. Safarnejad and F. Rasoulzadeh, *Bioimpacts*, 2016, **6**(3), 125.
49 V. S. Jisha, K. T. Arun, M. Hariharan and D. Ramaiah, *J. Am. Chem. Soc.*, 2006, **128**, 6024.
50 C. Cantor and P. R. Schimmel, *Biophysical Chemistry, part II*, W. H. Freeman and Company, San Francisco, 1980.
51 C. Michael and N. K. Puri, *Biochem. J.*, 1992, **282**, 589.
52 S. Das, Md. M. Islam, G. C. Jana, A. Patra, P. K. Jha and M. Hossain, *J. Mol. Recognit.*, 2017, e2609.